MULTISCALE MODEL. SIMUL.
Vol. 6, No. 1, pp. 228–245

STOCHASTIC SIMULATIONS FOR FLOW IN NONSTATIONARY RANDOMLY HETEROGENEOUS POROUS MEDIA USING A KL-BASED MOMENT-EQUATION APPROACH*

ZHIMING LU† AND DONGXIAO ZHANG‡

Abstract. In this study, we extend the Karhunen–Loève moment equation (KLME) approach, an approach based on KL decomposition, to efficiently and accurately quantify uncertainty for flow in nonstationary heterogeneous porous media that include a number of zones with different statistics of the hydraulic conductivity. We first decompose the log hydraulic conductivity $Y = \ln K_s$ for each zone by the KL decomposition, which is related to a set of eigenvalues and their corresponding orthogonal deterministic eigenfunctions. Based on the decomposition for all individual zones, we develop an algorithm to find the eigenvalues and eigenfunctions for the entire domain. Following the methodology proposed by Zhang and Lu [*J. Comput. Phys.*, 194 (2004), pp. 773–794], we solve the head variability up to second order in terms of σ_Y^2 and compare the results with those obtained from Monte Carlo (MC) simulations. It is evident that the results from the KLME approach with higher-order corrections are close to those from the MC simulations, but the computational cost for the KLME method is much lower than that for the MC simulations.

Key words. Karhunen–Loève moment equation, Monte Carlo simulations, moment-equation methods, Karhunen–Loève decomposition, nonstationary, heterogeneity, variability, porous media

AMS subject classifications. 60H15, 60H35, 65C05, 65C30, 76S05, 78M05, 82C31

DOI. 10.1137/060665282

1. Introduction.

Predicting flow and transport in porous media inevitably involves uncertainties because of our incomplete knowledge in hydraulic properties of these media. Such properties are conventionally treated as spatially random functions, and the equations governing flow and transport in such porous media are stochastic. In the last two decades, many predictive models have been developed to predict the mean flow and to quantify uncertainties associated with the mean predictions [6, 7, 5, 20]. Monte Carlo (MC) simulations and the moment-equation approach are two widely used methods for solving stochastic partial differential equations. However, both can be computationally expensive for large-scale problems [15].

Zhang and Lu [21] proposed an efficient and accurate Karhunen–Loève moment-equation (KLME) method for solving stochastic equations based on the KL decomposition of the stationary process, i.e, log hydraulic conductivity. Specifically, with the combination of the KL decomposition and perturbation methods, they evaluated the mean head up to fourth order in σ_Y and the head (co)variance up to third order in σ_Y^2. They also explored the validity of this approach for different degrees of medium variability and various correlation scales through comparisons against MC simulations. Lu and Zhang [15] systematically compared the KLME method with

*Received by the editors July 17, 2006; accepted for publication (in revised form) December 15, 2006; published electronically April 24, 2007.

http://www.siam.org/journals/mms/6-1/66528.html

†Hydrology and Geochemistry Group (EES-6), Earth and Environmental Sciences Division, MS T003, Los Alamos National Laboratory, Los Alamos, NM 87545 (zhiming@lanl.gov).

‡Mewbourne School of Petroleum and Geological Engineering, University of Oklahoma, 100 East Boyd, SEC T301, Norman, OK 73019 (donzhang@ou.edu).

MC simulations and the conventional moment-equation (CME) method in terms of computational efficiency and solution accuracy. They demonstrated that the KLME method is computationally much more efficient than both the MC simulations and the CME approach while retaining high accuracy (i.e., close to MC results).

The method has been applied to several different flow and solute transport scenarios, including fluid flow in unsaturated soils [19], two-phase (water and oil) flow [2, 3], fluid flow in unconfined systems [11], transient flow [17], and solute transport in saturated porous media [12]. It is assumed in all these studies that the porous media are stationary, which means that the mean hydraulic properties are constant in the domain and that the covariance between any two points in the simulation domain depends on their distance rather than the actual locations of these two points. However, hydraulic properties exhibit spatial variations at various scales, such as at the laboratory scale due to variations in pore geometry, at the field scale due to soil stratifications, and at the regional scale due to large-scale geological variability. Therefore, it is important to extend the KLME method for simulating flow and transport in random porous media with a multiscale variability.

Lu and Zhang [16] developed a conditional KLME method to incorporate permeability measurements in porous media. Conditioning renders the log hydraulic conductivity field statistically inhomogeneous (spatially nonstationary) for an otherwise stationary field. The algorithm is very efficient for some special problems in which the eigenvalues and eigenfunctions for the unconditional field can be solved analytically. In this study, our focus will be on development of an efficient strategy for predicting head moments for flow in randomly heterogeneous, two-scale porous media. The hydraulic conductivity of porous media varies spatially at a large scale as different zonations (due to stratifications, for example) and also at a smaller scale within each individual zone.

The remainder of this paper is organized as follows. We begin by describing the mathematical formulation for flow in heterogeneous porous media. We then present a detailed description of methodology for decomposing nonstationary random fields. For mathematical completeness, the KL-based moment equations are briefly provided. Finally, some numerical examples are used to validate the model by comparing with MC simulation results, followed by a short summary and discussion.

2. Stochastic differential equations. We consider transient water flow in saturated media satisfying the following continuity equation and Darcy's law [1],

$$S_s \frac{\partial h(\mathbf{x},t)}{\partial t} + \nabla \cdot \mathbf{q}(\mathbf{x},t) = g(\mathbf{x},t), \tag{2.1}$$

$$\mathbf{q}(\mathbf{x},t) = -K_s(\mathbf{x}) \nabla h(\mathbf{x},t), \tag{2.2}$$

subject to initial and boundary conditions:

$$h(\mathbf{x},0) = H_0(\mathbf{x}), \qquad \mathbf{x} \in \Omega, \tag{2.3}$$

$$h(\mathbf{x},t) = H(\mathbf{x},t), \qquad \mathbf{x} \in \Gamma_D, \tag{2.4}$$

$$\mathbf{q}(\mathbf{x},t) \cdot \mathbf{n}(\mathbf{x}) = Q(\mathbf{x},t), \qquad \mathbf{x} \in \Gamma_N, \tag{2.5}$$

where $\mathbf{q}$ is the flux, $h(\mathbf{x},t)$ is the hydraulic head, $H_0(\mathbf{x})$ is the initial head in the domain Ω, $H(\mathbf{x},t)$ is the prescribed head on Dirichlet boundary segments Γ_D, $K_s(\mathbf{x})$ is the saturated hydraulic conductivity, $Q(\mathbf{x},t)$ is the prescribed flux across Neumann

boundary segments Γ_N, $\mathbf{n}(\mathbf{x}) = (n_1, \ldots, n_d)^T$ is an outward unit vector normal to the boundary $\Gamma = \Gamma_D \cup \Gamma_N$, d is the dimension of the problem, and S_s is the specific storage. For simplicity, in this study, we assume that specific storage S_s and all boundary and initial conditions are deterministic, while $K_s(\mathbf{x})$ is treated as a random function, and thus (2.1)–(2.5) become stochastic partial differential equations, whose solutions are no longer deterministic values but probability distributions or related statistical moments. Our aim is to find the mean hydraulic head and its associated uncertainties.

Though the moment-equation approach is free of assumptions on parameter distributions, for the sake of comparison with the MC method, we assume that the hydraulic conductivity $K_s(\mathbf{x})$ in each zone follows a log normal distribution, and we work with the log-transformed variable $Y(\mathbf{x}) = \ln[K_s(\mathbf{x})] = \langle Y(\mathbf{x})\rangle + Y'(\mathbf{x})$, where $\langle Y(\mathbf{x})\rangle$ is the mean and $Y'(\mathbf{x})$ is the zero-mean fluctuation. The statistics (mean, variance, and correlation lengths) of the log hydraulic conductivity may be different for different zones. It is assumed that the log hydraulic conductivity in any zone is uncorrelated with that in all other zones [18, 14].

3. KL decomposition of the log hydraulic conductivity. The KL decomposition of a stationary conductivity field has been presented in literature [8, 9, 10, 21]. However, for completeness and convenience of presentation, the procedure is outlined here and followed by an algorithm for decomposing nonstationary fields. For a stochastic process $Y(\mathbf{x}) = \ln[K_s(\mathbf{x})]$, where $\mathbf{x} \in \Omega$ is the domain of interest, because its covariance function $C_Y(\mathbf{x}, \mathbf{y}) = \langle Y'(\mathbf{x})Y'(\mathbf{y})\rangle$ is bounded, symmetric, and positive definite, it can be decomposed into [4]

$$C_Y(\mathbf{x}, \mathbf{y}) = \sum_{n=1}^{\infty} \lambda_n f_n(\mathbf{x}) f_n(\mathbf{y}), \tag{3.1}$$

where λ_n are eigenvalues and $f_n(\mathbf{x})$ are orthogonal, deterministic functions that form a complete set [13],

$$\int_\Omega f_n(\mathbf{x}) f_m(\mathbf{x}) d\mathbf{x} = \delta_{nm}, \qquad n, m \geq 1, \tag{3.2}$$

where δ_{nm} is the Kronecker delta function, $\delta_{nm} = 1$ for $n = m$, and $\delta_{nm} = 0$ otherwise. The mean-removed stochastic process $Y'(\mathbf{x})$ can be expanded in terms of λ_n and $f_n(\mathbf{x})$ as

$$Y'(\mathbf{x}) = \sum_{n=1}^{\infty} \xi_n \sqrt{\lambda_n} f_n(\mathbf{x}), \tag{3.3}$$

where ξ_n are orthogonal random variables, i.e., $\langle \xi_n \rangle = 0$ and $\langle \xi_n \xi_m \rangle = \delta_{nm}$. Under the assumption that $Y(\mathbf{x})$ is normally distributed, ξ_n are orthogonal standard Gaussian random variables. The expansion in (3.3) is called the KL expansion. The eigenvalues and eigenfunctions can be solved from the following Fredholm equation:

$$\int_\Omega C_Y(\mathbf{x}, \mathbf{y}) f(\mathbf{y}) d\mathbf{y} = \lambda f(\mathbf{x}). \tag{3.4}$$

This equation can be solved analytically for some special cases, such as in the case of a rectangular domain with a separable exponential covariance function [21]. In general, however, (3.4) has to be solved numerically. Ghanem and Spanos [8] presented a

Galerkin-type algorithm for solving (3.4), which involves solving an eigenvalue problem $C\mathbf{X} = \lambda\mathbf{X}$, where C is an $N \times N$ matrix, $\mathbf{X}$ is a vector of size N, and N is the number of grid nodes in the domain Ω. The summation of all eigenvalues can be determined by setting $\mathbf{y} = \mathbf{x}$ in (3.1) and integrating the derived equation with respect to $\mathbf{x}$ over Ω, which yields $\sum_{n=1}^{\infty} \lambda_n = \sigma_Y^2 |\Omega|$, where $|\Omega|$ is the size of the flow domain (an area for two-dimensional problems and a volume for three-dimensional problems).

Note that stationarity of the process $Y(\mathbf{x})$ is not required in the above procedure. Suppose the simulation domain is partitioned into M nonoverlapping subdomains $\Omega = \bigcup_{m=1}^{M} \Omega_m$ and $\Omega_m \cap \Omega_n = \phi$ for $m \neq n$, and accordingly the log hydraulic conductivity field can be written as

$$Y(\mathbf{x}) = \ln K_s(\mathbf{x}) = \sum_{m=1}^{M} Y_m(\mathbf{x})\psi_m(\mathbf{x}), \tag{3.5}$$

where $Y_m(\mathbf{x}) = \ln K_s(\mathbf{x})$ is a spatial random function defined in subdomain Ω_m, and $\psi_m(\mathbf{x})$ is a deterministic indicator function given as $\psi_m(\mathbf{x}) = 1$ for $\mathbf{x} \in \Omega_m$ and $\psi_m(\mathbf{x}) = 0$ otherwise. For convenience in mathematical representation, $Y_m(\mathbf{x})$ is extended to the entire domain Ω as $Y_m(\mathbf{x}) = 0$ for $\mathbf{x} \notin \Omega_m$. From (3.5), one can derive the mean, perturbation, and covariance of $Y(\mathbf{x})$ as [14]

$$\langle Y(\mathbf{x})\rangle = \sum_{m=1}^{M} \langle Y_m(\mathbf{x})\rangle\psi_m(\mathbf{x}), \tag{3.6}$$

$$Y'(\mathbf{x}) = \sum_{m=1}^{M} Y'_m(\mathbf{x})\psi_m(\mathbf{x}), \tag{3.7}$$

and

$$C_Y(\mathbf{x}, \mathbf{y}) = \sum_{m=1}^{M} C_m(\mathbf{x}, \mathbf{y})\psi_m(\mathbf{x})\psi_m(\mathbf{y}), \tag{3.8}$$

where $C_m(\mathbf{x}, \mathbf{y}) = 0$ for $\mathbf{x} \notin \Omega_m$ or $\mathbf{y} \notin \Omega_m$. By definition, the eigenvalues and eigenfunctions for the entire domain Ω have to satisfy (3.4). Substituting (3.8) into (3.4) yields

$$\sum_{m=1}^{M} \psi_m(\mathbf{x}) \int_{\Omega_m} C_m(\mathbf{x}, \mathbf{y}) f(\mathbf{y}) d\mathbf{y} = \lambda f(\mathbf{x}). \tag{3.9}$$

For any $\mathbf{x} \in \Omega_m$, (3.9) leads to

$$\int_{\Omega_m} C_m(\mathbf{x}, \mathbf{y}) f(\mathbf{y}) d\mathbf{y} = \lambda f(\mathbf{x}), \tag{3.10}$$

which means that eigenvalues and eigenfunctions for the entire domain Ω must be the eigenvalues and eigenfunctions in each individual subdomain. Note that the solution of (3.10) includes infinity numbers of eigenvalues and eigenfunctions. Suppose we have solved eigenvalues $\lambda_n^{(m)}$ and eigenfunctions $f_n^{(m}(\mathbf{x})$, $n = 1, 2, \ldots$, from (3.10) for all subdomain Ω_m, $m = \overline{1, M}$. These eigenfunctions $f_n^{(m)}(\mathbf{x})$ are defined only on the

subdomain Ω_m and are then extended to the entire domain Ω such that $f_n^{(m)}(\mathbf{x}) = 0$ for $\mathbf{x} \notin \Omega_m$, $m = \overline{1, M}$, $n = 1, 2, \ldots$. From the above reasoning, it is easy to see that the sets $\lambda_n^{(m)}$ and $f_n^{(m)}(\mathbf{x})$, $m = \overline{1, M}$, $n = 1, 2, \ldots$, are the eigenvalues and eigenfunctions for the domain Ω, which leads to the following decomposition of Y':

$$Y'(\mathbf{x}) = \sum_{m=1}^{M} \sum_{n=1}^{\infty} \zeta_n^{(m)} \sqrt{\lambda_n^{(m)}} f_n^{(m)}(\mathbf{x}), \tag{3.11}$$

where $\zeta_n^{(m)}$ are orthogonal random variables with a zero mean and unit variance, and the indicator function $\psi_m(\mathbf{x})$ in (3.11) has been dropped because $f_n^{(m)}(\mathbf{x})$ is also zero for $\mathbf{x} \notin \Omega_m$.

Since the decomposition of $Y'(\mathbf{x})$ includes an infinite number of terms, one has to truncate the series in (3.11). Because the magnitudes of $\lambda_n^{(m)}$ are related to the size of the subdomain Ω_m and the variability $\sigma_{Y,m}^2$ by $\sum_n \lambda_n^{(m)} = \sigma_{Y,m}^2 |\Omega_m|$, where $|\Omega_m|$ is the size of subdomain Ω_m, one may need to sort $\lambda_n^{(m)}$ before truncating the decomposition in (3.11). After sorting and rearranging its terms, (3.11) may be written formally as

$$Y'(\mathbf{x}) = \sum_{k=1}^{\infty} \xi_k \sqrt{\lambda_k} f_k(\mathbf{x}), \tag{3.12}$$

where λ_k and $f_k(\mathbf{x})$ are eigenvalues and eigenfunctions for the entire domain. The procedure can be summarized as follows:

1. Equation (3.10) is solved for each individual zone Ω_m to obtain eigenvalues $\{\lambda_n^{(m)}, n = 1, 2, \ldots\}$ and eigenfunctions $\{f_n^{(m)}(\mathbf{x}), n = 1, 2, \ldots\}$.
2. Extend the domain of $f_n^{(m)}(\mathbf{x})$ from Ω_m to Ω by defining $f_n^{(m)}(\mathbf{x}) = 0$ for $\mathbf{x} \notin \Omega_m$.
3. Merge M sets of eigenvalues $\{\lambda_n^{(m)}, m = \overline{1, M}, n = 1, 2, \ldots\}$ and sort them in a nonincreasing order (denoting the sorted series as λ_k, $k = 1, 2, \ldots$).
4. Arrange the set of merged eigenfunctions $\{f_n^{(m)}, m = \overline{1, M}, n = 1, 2, \ldots\}$ based on the sorted eigenvalues and denote the new set of eigenfunctions as $f_k(\mathbf{x})$, $k = 1, 2, \ldots$.

One can easily see that λ_k and $f_k(\mathbf{x})$ satisfy (3.4). In addition, it can be shown that the set of eigenfunctions $f_k(\mathbf{x})$ is orthogonal. In fact, if f_i and f_j originally (before merging and sorting) belong to the same group m solved from (3.10), say, $f_n^{(m)}$ and $f_k^{(m)}$, by definition and noting that $f_n^{(m)}(\mathbf{x})$ and $f_k^{(m)}(\mathbf{x})$ are zero for $\mathbf{x} \notin \Omega_m$, one has

$$\int_{\Omega} f_i(\mathbf{x}) f_j(\mathbf{x}) d\mathbf{x} = \int_{\Omega_m} f_n^{(m)}(\mathbf{x}) f_k^{(m)}(\mathbf{x}) d\mathbf{x} = \delta_{nk}, \tag{3.13}$$

which is identical to δ_{ij} because $i = j$ if and only if $n = k$. On the other hand, if f_i and f_j are from two different groups, say, $f_n^{(m)}$ and $f_k^{(l)}$, $m \neq l$, one has

$$\int_{\Omega} f_i(\mathbf{x}) f_j(\mathbf{x}) d\mathbf{x} = \int_{\Omega} f_n^{(m)}(\mathbf{x}) f_k^{(l)}(\mathbf{x}) d\mathbf{x} = 0, \tag{3.14}$$

because of the fact that $f_n^{(m)}(\mathbf{x})$ is nonzero only for $\mathbf{x} \in \Omega_m$, while $f_k^{(l)}(\mathbf{x})$ is nonzero only for $\mathbf{x} \in \Omega_l$.

The KL decomposition provides a way to generate realizations. Once the eigenvalues λ_k and their corresponding eigenfunctions f_k are solved, realizations of the log hydraulic conductivity field can be generated simply by independently sampling a certain number of values z_k from the standard Gaussian distribution $N(0,1)$ and then computing

$$Y(\mathbf{x}) \approx \sum_{m=1}^{M} \langle Y_m(\mathbf{x})\rangle \psi_m(\mathbf{x}) + \sum_{k=1}^{K} z_k \sqrt{\lambda_k} f_k(\mathbf{x}), \tag{3.15}$$

where K is the number of terms needed to generate realizations with a given accuracy. This equation will be used to generate a number of MC realizations for the purpose of verifying the accuracy of the KLME method, as discussed in illustrative examples.

Since eigenvalues $\sqrt{\lambda_k}$ and their corresponding eigenfunctions $f_k(\mathbf{x})$ always appear together, in the following derivations, we define new functions $\tilde{f}_k(\mathbf{x}) = \sqrt{\lambda_k} f_k(\mathbf{x})$, and the tilde over f_k is dropped for simplicity.

4. KL-based moment equations. Since the dependent variable $h(\mathbf{x},t)$ is a function of the input variability $\sigma_Y^2(\mathbf{x})$, one may express $h(\mathbf{x},t)$ as an infinite series as $h(\mathbf{x},t) = \sum_{m=1}^{\infty} h^{(m)}(\mathbf{x},t)$. In this series, the order of each term is with respect to $\sigma_Y(\mathbf{x})$. We also expand $K_s(\mathbf{x}) = \exp[Y(\mathbf{x})] = \exp[\langle Y(\mathbf{x})\rangle + Y'(\mathbf{x})] = K_G(\mathbf{x})[1 + Y' + (Y')^2/2 + \cdots]$, where $K_G(\mathbf{x})$ is the geometric mean of the saturated hydraulic conductivity K_s. After combining (2.1) and (2.2), substituting expansions of $h(\mathbf{x},t)$ and $K_s(\mathbf{x})$ into resultant equations, and collecting terms at separate orders, we obtain

$$\nabla \cdot \Big[K_G(\mathbf{x}) \nabla h^{(0)}(\mathbf{x},t)\Big] + g(\mathbf{x},t) = S_s \frac{\partial h^{(0)}(\mathbf{x},t)}{\partial t}, \tag{4.1}$$

$$h^{(0)}(\mathbf{x},0) = H_0(\mathbf{x}), \qquad \mathbf{x} \in \Omega, \tag{4.2}$$

$$h^{(0)}(\mathbf{x},t) = H_1(\mathbf{x},t), \qquad \mathbf{x} \in \Gamma_D, \tag{4.3}$$

$$-K_G(\mathbf{x}) \nabla h^{(0)}(\mathbf{x},t) \cdot \mathbf{n}(\mathbf{x}) = Q(\mathbf{x},t), \qquad \mathbf{x} \in \Gamma_N, \tag{4.4}$$

and, for $m \geq 1$,

$$\nabla \cdot \Big[K_G(\mathbf{x}) \nabla h^{(m)}(\mathbf{x},t)\Big] + g^{(m)}(\mathbf{x},t) = S_s \frac{\partial h^{(m)}(\mathbf{x},t)}{\partial t}, \tag{4.5}$$

$$h^{(m)}(\mathbf{x},0) = 0, \qquad \mathbf{x} \in \Omega, \tag{4.6}$$

$$h^{(m)}(\mathbf{x},t) = 0, \qquad \mathbf{x} \in \Gamma_D, \tag{4.7}$$

$$K_G(\mathbf{x}) \nabla h^{(m)}(\mathbf{x},t) \cdot \mathbf{n}(\mathbf{x}) = (-1)^{m+1} \frac{Q(\mathbf{x},t)}{m!} [Y'(\mathbf{x})]^m, \qquad \mathbf{x} \in \Gamma_N, \tag{4.8}$$

where

$$\begin{aligned} g^{(m)}(\mathbf{x},t) = &- S_s \sum_{k=1}^{m} \frac{(-1)^k}{m!} [Y'(\mathbf{x})]^k \frac{\partial h^{(m-k)}(\mathbf{x},t)}{\partial t} \\ &+ K_G(\mathbf{x}) \nabla Y'(\mathbf{x}) \cdot \nabla h^{(m-1)}(\mathbf{x},t) + \frac{g(\mathbf{x},t)}{m!} [-Y'(\mathbf{x})]^m. \end{aligned} \tag{4.9}$$

Equations (4.1)–(4.4) are the governing equations for the zeroth-order mean head. In the CME approach, the equations for higher-order corrections (usually up to second order) for the mean head are obtained from (4.5)–(4.9). For example, the second-order correction $\langle h^{(2)}(\mathbf{x},t)\rangle$ can be derived by setting $m=2$ in (4.5)–(4.9), taking the ensemble mean of these equations, and solving the derived moment equations. The first-order (in terms of σ_Y^2) head covariance can be derived from (4.5)–(4.9) by setting $m=1$, multiplying the derived equation for $h^{(1)}(\mathbf{x},t)$ by $h^{(1)}(\boldsymbol{\chi},\tau)$, and taking the ensemble mean. As demonstrated in [15], the CME approach is computationally expensive, especially for higher-order solutions in large-scale problems.

In the KLME method, we further assume that $h^{(m)}(\mathbf{x},t)$ can be expanded in terms of those orthogonal random variables ξ_n, $n=1,2,\ldots$, which are used in expanding $Y'(\mathbf{x})$ [21],

$$h^{(m)}(\mathbf{x},t)=\sum_{i_1,i_2,\ldots,i_m=1}^{\infty}\left(\prod_{j=1}^{m}\xi_{i_j}\right)h^{(m)}_{i_1,i_2,\ldots,i_m}(\mathbf{x},t), \tag{4.10}$$

for example,

$$h^{(1)}=\sum_{i=1}^{\infty}h^{(1)}_i\xi_i,\quad h^{(2)}=\sum_{i,j=1}^{\infty}h^{(2)}_{ij}\xi_i\xi_j,\quad h^{(3)}=\sum_{i,j,k=1}^{\infty}h^{(3)}_{ijk}\xi_i\xi_j\xi_k, \tag{4.11}$$

where $h^{(m)}_{i_1,i_2,\ldots,i_m}(\mathbf{x},t)$ are deterministic functions to be determined. Substituting decomposition of $Y'(\mathbf{x})$, i.e., (3.3), and, recursively, $h^{(m)}(\mathbf{x},t)$ into (4.5)–(4.9), we obtain governing equations for $h^{(m)}_{i_1,i_2,\ldots,i_m}$. For example, substituting decompositions of $Y'(\mathbf{x})$ and $h^{(1)}(\mathbf{x},t)$ into (4.5)–(4.9) for $m=1$, one derives equations for $\{h^{(1)}_n\}$ that include infinite series in terms of $\{\xi_n\}$. Because of the orthogonality of set $\{\xi_n\}$, by multiplying ξ_k on the resultant equations and taking the ensemble mean, one obtains the equation and initial and boundary conditions for each individual term $h^{(1)}_n$, which read as

$$\nabla\cdot\left[K_G(\mathbf{x})\nabla h^{(1)}_n(\mathbf{x},t)\right]+g^{(1)}_n(\mathbf{x},t)=S_s\frac{\partial h^{(1)}_n(\mathbf{x},t)}{\partial t}, \tag{4.12}$$

$$h^{(1)}_n(\mathbf{x},0)=0,\qquad \mathbf{x}\in D, \tag{4.13}$$

$$h^{(1)}_n(\mathbf{x},t)=0,\qquad \mathbf{x}\in\Gamma_D, \tag{4.14}$$

$$K_G(\mathbf{x})\nabla h^{(1)}_n(\mathbf{x},t)\cdot\mathbf{n}(\mathbf{x})=Q(\mathbf{x},t)f_n(\mathbf{x}),\qquad \mathbf{x}\in\Gamma_N, \tag{4.15}$$

where

$$g^{(1)}_n(\mathbf{x},t)=\left[S_s\frac{\partial h^{(0)}(\mathbf{x},t)}{\partial t}-g(\mathbf{x},t)\right]f_n(\mathbf{x})+K_G(\mathbf{x})\nabla f_n(\mathbf{x})\cdot\nabla h^{(0)}(\mathbf{x},t). \tag{4.16}$$

Recalling the definition of $f_n(\mathbf{x})$, it is seen that all driving terms in (4.12)–(4.16) are proportional to $\sqrt{\lambda_n}$, which decreases as n increases. This ensures that the magnitude of contribution of $h^{(1)}_n(\mathbf{x},t)$ to $h^{(1)}(\mathbf{x},t)$ decreases with n in general. This also clearly indicates that $h^{(1)}_n(\mathbf{x},t)$ are proportional to $\sigma_Y(\mathbf{x})$. Derivation of higher-order terms $h^{(m)}_{i_1,i_2,\ldots,i_m}(\mathbf{x},t)$ can be found in [21].

We solve $h^{(m)}_{i_1,i_2,\ldots,i_m}$ up to third order, i.e., $m = 3$. Once we solve $h^{(0)}$, $h^{(1)}_n$, $h^{(2)}_{ij}$, and $h^{(3)}_{ijk}$, we can directly compute the mean head and the head covariance without solving equations for $C_h(\mathbf{x}, t; \boldsymbol{\chi}, \tau)$ and $C_{Yh}(\mathbf{x}; \boldsymbol{\chi}, \tau)$, both of which are required in the CME approach. Up to third order in σ_Y, the head is approximated by

$$h(\mathbf{x}, t) \approx \sum_{i=0}^{3} h^{(i)}(\mathbf{x}, t), \tag{4.17}$$

which leads to an expression for the mean head

$$\langle h(\mathbf{x}, t)\rangle \approx \sum_{i=0}^{3} \langle h^{(i)}(\mathbf{x}, t)\rangle = h^{(0)}(\mathbf{x}, t) + \sum_{i=1}^{\infty} h^{(2)}_{ii}(\mathbf{x}, t). \tag{4.18}$$

The first term on the right-hand side of (4.18) is the zeroth-order (or first-order) approximation of the mean head: $\langle h^{(0)}(\mathbf{x}, t)\rangle \equiv h^{(0)}(\mathbf{x}, t)$. The second term represents the second-order (or third-order) correction to the zeroth-order mean head. In deriving (4.18), we used the fact $\langle \xi_i \xi_j \rangle = \delta_{ij}$.

From (4.17)–(4.18), one can write the head perturbation up to third-order accuracy,

$$h'(\mathbf{x}, t) = h(\mathbf{x}, t) - \langle h(\mathbf{x}, t)\rangle \approx \sum_{i=1}^{3} h^{(i)}(\mathbf{x}, t) - \langle h^{(2)}(\mathbf{x}, t)\rangle, \tag{4.19}$$

where $\langle h^{(2)}\rangle = \langle \sum_{i,j=1}^{\infty} \xi_i \xi_j h^{(2)}_{ij}\rangle = \sum_{i=1}^{\infty} h^{(2)}_{ii}$. Equation (4.19) leads to the head covariance

$$\begin{aligned} C_h(\mathbf{x}, t; \mathbf{y}, \tau) = {} & \sum_{i=1}^{\infty} h^{(1)}_i(\mathbf{x}, t) h^{(1)}_i(\mathbf{y}, \tau) + 2 \sum_{i,j=1}^{\infty} h^{(2)}_{ij}(\mathbf{x}, t) h^{(2)}_{ij}(\mathbf{y}, \tau) \\ & + 3 \sum_{i,j=1}^{\infty} h^{(1)}_i(\mathbf{x}, t) h^{(3)}_{ijj}(\mathbf{y}, \tau) + 3 \sum_{i,j=1}^{\infty} h^{(1)}_i(\mathbf{y}, \tau) h^{(3)}_{ijj}(\mathbf{x}, t). \end{aligned} \tag{4.20}$$

The head variance up to second order in σ_Y^2 (or fourth order in σ_Y) can be derived from (4.20) as

$$\sigma^2_h(\mathbf{x}, t) = \sum_{i=1}^{\infty} [h^{(1)}_i(\mathbf{x}, t)]^2 + 2 \sum_{i,j=1}^{\infty} [h^{(2)}_{ij}(\mathbf{x}, t)]^2 + 6 \sum_{i,j=1}^{\infty} h^{(1)}_i(\mathbf{x}, t) h^{(3)}_{ijj}(\mathbf{x}, t). \tag{4.21}$$

Here the first term on the right-hand side of (4.21) represents the head variance up to first order in σ_Y^2, and the second and third terms are second-order (in σ_Y^2) corrections. Note that, using the CME method, one can solve only the first term in (4.21) at the cost of solving sets of algebraic equations with N unknowns for about $2N$ times, where N is the number of grid nodes in the domain.

5. Illustrative examples. In this section, we attempt to examine the validity of the KL-based moment-equation approach in computing higher-order head moments for flow in hypothetical, zoned saturated porous media by comparing model results with those from MC simulations.

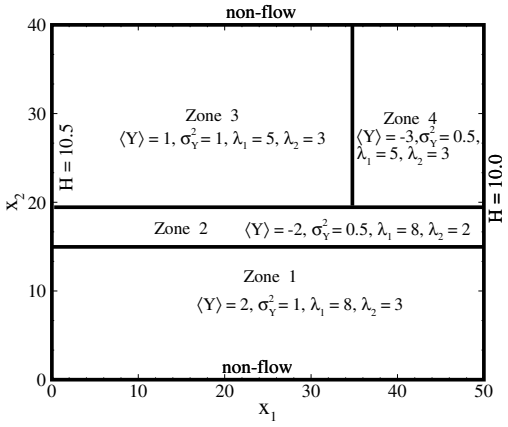

FIG. 5.1. *Schematic diagram showing the zonation and the boundary configuration for case* 1.

In the first example (case 1), we consider a two-dimensional domain in a saturated heterogeneous porous medium. A rectangular flow domain of size $L_1 = 50$ $[L]$ and $L_2 = 40$ $[L]$ (where L is any consistent length unit) is partitioned into four zones and uniformly discretized into 50×40 square elements (Figure 5.1). The hydraulic head is prescribed at the left and right boundaries as 10.5 $[L]$ and 10.0 $[L]$, respectively. The no-flow conditions are prescribed at two lateral boundaries. The statistics of medium properties for all zones are also shown in Figure 5.1.

The log saturated hydraulic conductivity $Y(\mathbf{x}) = \ln K_s(\mathbf{x})$ in each zone Ω_m is second-order stationary with a separable exponential covariance function,

$$C_Y^{(m)}(\mathbf{x},\mathbf{y}) = C_Y^{(m)}(x_1,x_2;y_1,y_2) = \sigma_{Y,m}^2 \exp\left[-\frac{|x_1-y_1|}{\eta_1^{(m)}} - \frac{(|x_2-y_2|)}{\eta_2^{(m)}}\right], \tag{5.1}$$

where $\eta_1^{(m)}$ and $\eta_2^{(m)}$ are correlation lengths in the x_1- and x_2-directions, respectively, and may vary from zone to zone. In this case, the eigenvalues $\lambda_n^{(m)}$, $n = 1, 2, \ldots$, and their corresponding eigenfunctions $f_n^{(m)}(\mathbf{x})$, $n = 1, 2, \ldots$, for each zone Ω_m can be solved analytically [21]. For the entire domain, its eigenvalues and eigenfunctions can be obtained either by numerically solving (3.4) directly or solving (3.10) for each zone and then combining them together, as described in the previous sections. The two procedures lead to almost identical results. Note that, for a large-scale problem, solving the eigenvalue problem for the entire domain is computationally expensive, and solving it for each individual subdomain will significantly reduce the computational cost.

Figure 5.2 depicts eigenvalues for each zone and their accumulative eigenvalues as functions of the mode number. The maximum accumulative eigenvalue for each zone can be determined by the product of the variability of the log hydraulic conductivity and the size (area for the two-dimensional problem) of the subdomain. Note that, although theoretically the solution of (3.10) includes an infinite number of eigenvalues and eigenfunctions, the discretized version of the equation has a finite number of eigenvalues and eigenfunctions, which is the number of grid nodes in each zone. Short curves in the figure represent fewer grid nodes in their corresponding subdomains. Once the eigenvalues and eigenfunctions for each individual zone are solved,

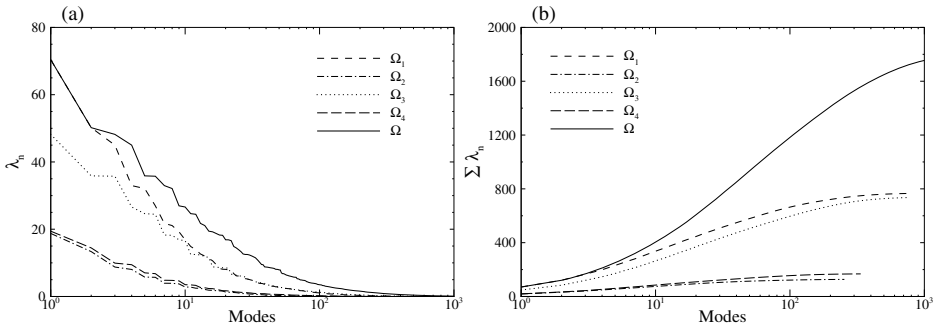

FIG. 5.2. *Eigenvalues* (a) *and the accumulative values* (b) *for four individual zones and the entire simulation domain for case* 1.

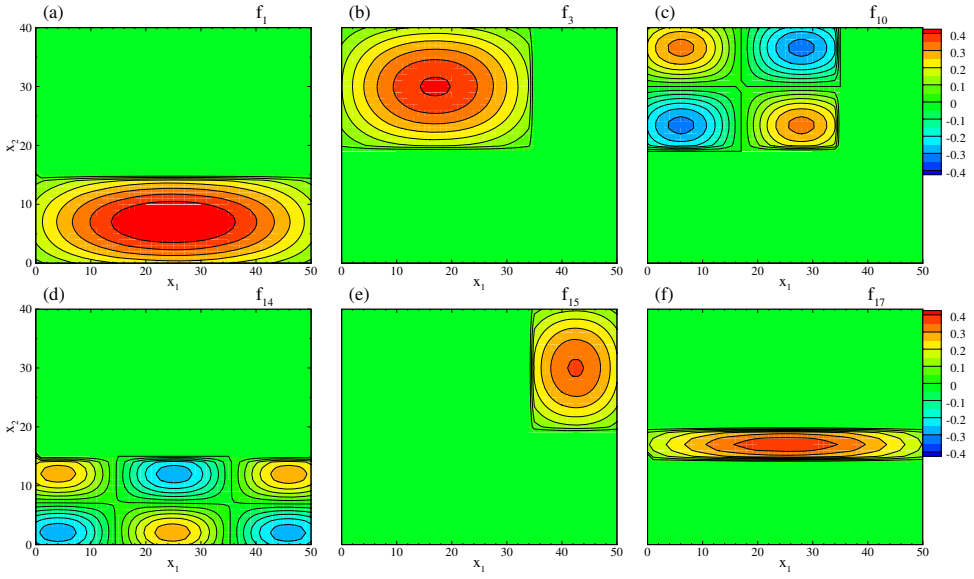

FIG. 5.3. *Selected eigenfunctions for case* 1.

the eigenvalues and eigenfunctions for the entire domain Ω can be determined using the algorithm described in section 4. The eigenvalues for the entire domain and its corresponding accumulative value are also illustrated in Figure 5.2. Some selected eigenfunctions for the entire domain are demonstrated in Figure 5.3.

Since the sum of all eigenvalues for any zone Ω_m is related to total variability $\sum \lambda_n = \sigma^2_{Y,m}|\Omega_m|$, the zone with either a small variability or a small size will have small magnitudes of $\lambda_n^{(m)}$ and will be ranked low in the sorted eigenvalues for the entire domain. As a result, the variability of the log hydraulic conductivity for such a zone will have a relatively small contribution to the statistics of the head field in the entire domain.

In this example, we choose $n_1 = 100$, $n_2 = 20$, and $n_3 = 10$, i.e., solving $h_i^{(1)}$ for $i = \overline{1, n_1}$, $h_{ij}^{(2)}$ for $i, j = \overline{1, n_2}$, and $h_{ijk}^{(3)}$ for $i, j, k = \overline{1, n_3}$. Because these terms are

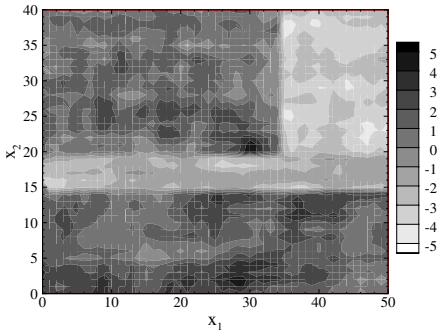

FIG. 5.4. *A typical MC realization of the log hydraulic conductivity field for case* 1.

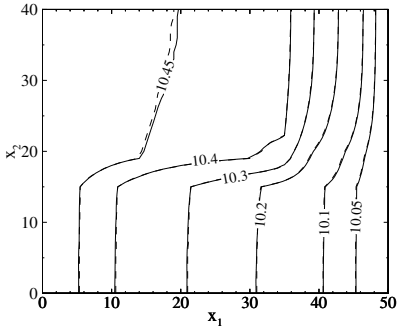

FIG. 5.5. *Comparison of the mean head fields from MC simulations (solid curves) and the KLME method up to zeroth-order (dashed curves) and second-order (dotted curves) accuracy for case* 1.

symmetric with respect to their indices, the actual number of times to solve sets of linear algebraic equations with N unknowns is 1 (zeroth order) + 100 (first order) + 220 (second order) + 230 (third order) = 551. The computational cost for solving each set of these equations is more or less equivalent to that for solving each of the MC realizations.

To demonstrate the accuracy and efficiency of the KLME method, we conducted MC simulations. MC realizations are generated using (3.15) based on the computed eigenvalues and eigenfunctions. Figure 5.4 shows a typical MC realization of the log hydraulic conductivity. Note that the range of the natural log hydraulic conductivity in this realization is about $-5.0 \sim 5.0$, which means that the difference of the hydraulic conductivity is about four orders of magnitude. The statistics (mean, variance, and correlation lengths) of the generated 10,000 realizations have been compared with their specified values. Each realization of the conductivity field is then used to solve the head field from the original flow equation with boundary and initial conditions, i.e., (2.1)–(2.5), and the statistics (mean and variance) of the hydraulic head are computed from the ensemble of these head realizations and are considered as the "true" solutions for the problem.

Figure 5.5 compares the mean head computed from MC simulations (solid curves) and the KLME method with zeroth-order (dashed curves) and second-order (dotted

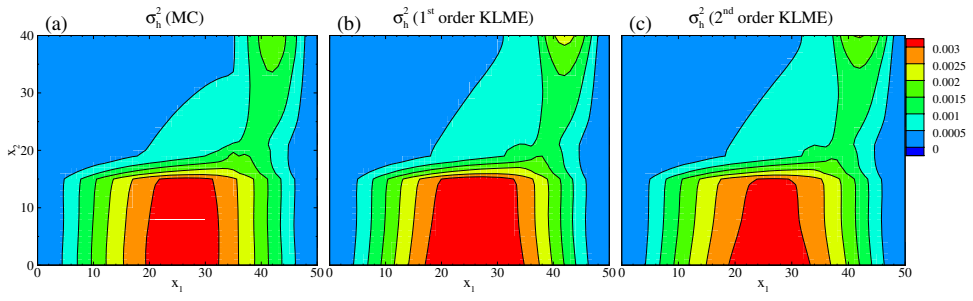

FIG. 5.6. *Comparison of the head variance from MC simulations and the KLME method up to second-order accuracy for case* 1.

curves) approximations. Here the zeroth-order solution represents the first term on the right-hand-side of (4.18), while the second-order solution accounts for both two terms (truncated series). For this particular case, although adding the second-order correction improves the solution slightly (the dotted curves are almost overlapped with the solid curves), the zeroth-order solution is fairly close to the MC results. Note that, because of relatively low hydraulic conductivity in Zone 4, the head gradient in this zone is large, while the gradient in Zone 3 is very low. This spatial pattern of the head gradient has a significant effect on head variability, as illustrated in Figure 5.6. The contour maps in Figure 5.6 compare the head variance derived from MC simulations and from the KLME method with first-order accuracy (truncated series of the first summation in (4.21)) and second-order accuracy (truncated series of all three summations in (4.21)) in terms of σ_Y^2. It is seen from the figure that both the first- and second-order approximations reproduce the MC results very well. In addition, it is worthy to note the spatial variation of the head variability over the domain. Zone 1 has the largest head variability, largely due to its high variability in the log hydraulic conductivity ($\sigma_{Y,1}^2 = 1.0$). Although Zone 3 has the same variability of the log hydraulic conductivity, the head variability is very low because of a low mean head gradient in this zone (see Figure 5.5). Zone 4 has a relative high head variability because of a high head gradient in this zone, but the head variability is smaller than that in Zone 1 due to a smaller variability in hydraulic conductivity ($\sigma_{Y,4}^2 = 0.5$).

In the second example (case 2), the simulation domain and flow boundary configuration are the same as in case 1, but the domain is partitioned into six zones, as illustrated in Figure 5.7. The proportions of different zones and the statistics of medium properties for all zones are listed in Table 5.1. The log saturated hydraulic conductivity $Y(\mathbf{x}) = \ln K_s(\mathbf{x})$ in each zone is second-order stationary with an exponential covariance function

$$C_Y(\mathbf{x}, \mathbf{y}) = C_Y(x_1, x_2; y_1, y_2) = \sigma_Y^2 \exp\left[-\frac{(x_1 - y_1)^2}{\eta_1^2} - \frac{(x_2 - y_2)^2}{\eta_2^2}\right]. \tag{5.2}$$

In this example, the eigenvalues $\lambda_n^{(m)}$, $n = 1, 2, \ldots$, and their corresponding eigenfunctions $f_n^{(m)}(\mathbf{x})$, $n = 1, 2, \ldots$, for each zone Ω_m have to be solved numerically from (3.10). Figure 5.8 illustrates the eigenvalues and their accumulative values for all six individual zones and the entire simulation domain. From the figure, it is seen that for the entire domain the first 100 modes account for about 76% of the total variability and the first 30 modes for about 50% of the total variability. Figure 5.9 depicts some selected eigenfunctions for the simulation domain.

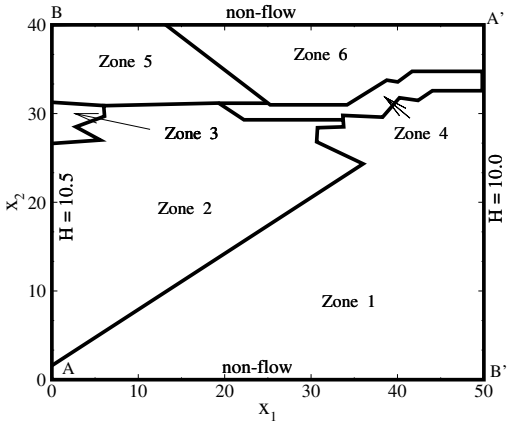

FIG. 5.7. *Schematic diagram showing the zonation and the boundary configuration for case* 2.

TABLE 5.1
Statistical parameters for different zones (case 2*).*

Parameters	Zone 1	Zone 2	Zone 3	Zone 4	Zone 5	Zone 6
Proportion	0.440	0.307	0.010	0.023	0.095	0.125
$\langle Y \rangle$	0.0	2.0	−2.0	−5.0	3.0	1.0
σ_Y^2	1.0	1.0	0.5	0.5	1.0	1.0
η_1	10.0	10.0	3.0	4.0	8.0	8.0
η_2	5.0	2.0	2.0	2.0	3.0	3.0
$\sum_n \lambda_n^{(m)}$	880.1	613.1	10.0	23.3	189.4	249.6

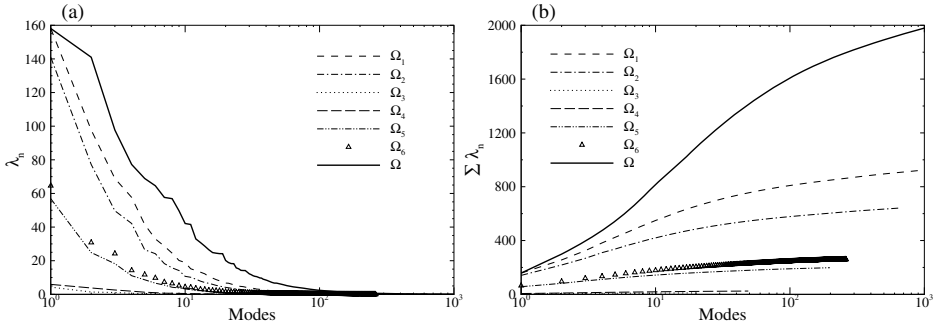

FIG. 5.8. *Eigenvalues* (a) *and the accumulative value* (b) *for six individual zones and the entire simulation domain for case* 2.

In this base case, we choose $n_1 = 100$, $n_2 = 20$, and $n_3 = 10$, requiring us to solve sets of linear algebraic equations with N unknowns for 551 times.

Figure 5.10 compares contour maps of the mean head computed from MC simulations (solid curves) and the KLME method with different orders of approximations. The figure demonstrates that, although the zeroth-order solution (dashed curves) is fairly close to the MC results, adding second-order corrections (dotted curves) does

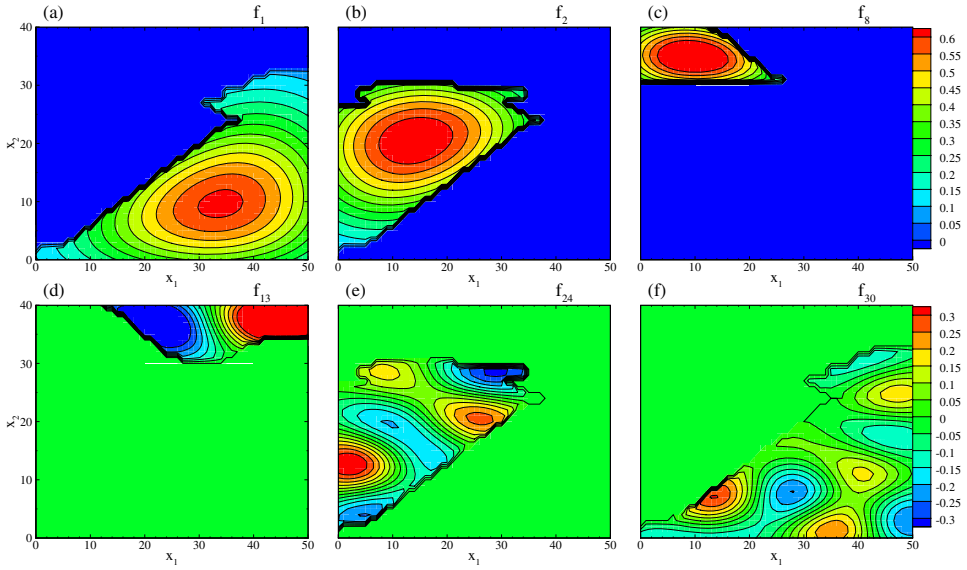

FIG. 5.9. *Selected eigenfunctions for case* 2.

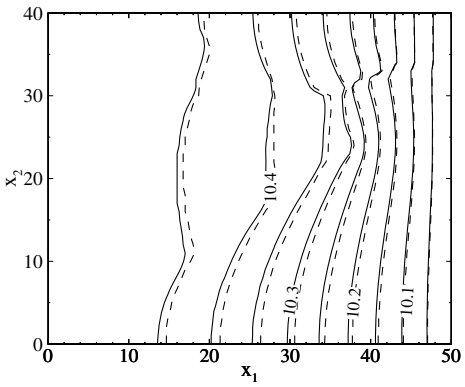

FIG. 5.10. *Comparison of the mean head from MC simulations and the KLME method up to second-order accuracy for case* 2.

improve the results significantly. In fact, the contours for the second-order mean head are almost identical to those of MC simulations.

The comparison of head variability derived from MC simulations and the KLME approach with different orders of approximations is illustrated in Figure 5.11. The figure shows that both first- and second-order approximations (in terms of σ_Y^2) reproduce MC results very well, while the computational cost for the KLME method is significantly lower than that required for MC simulations. It should be emphasized that, for the first-order KLME solution, the number of times needed to solve sets of linear algebraic equations of N (the number of grid nodes) unknowns is 101 for this case, as compared to thousands of times for the MC simulations and $2N$ times for the CME method [15]. Next, we explore in some detail how the number of terms in-

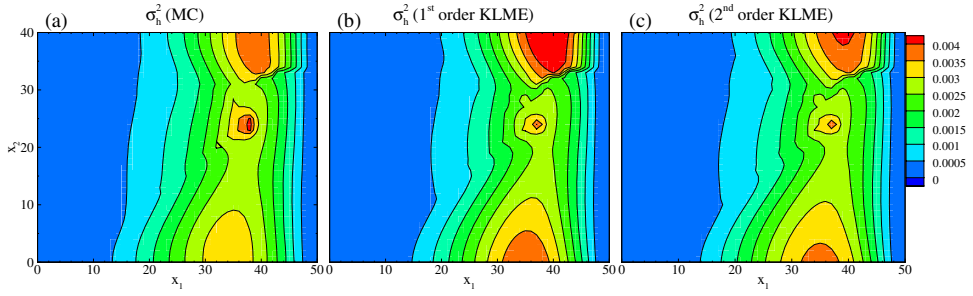

FIG. 5.11. *Comparison of the head variance from MC simulations and the KLME method up to second-order accuracy for case* 2.

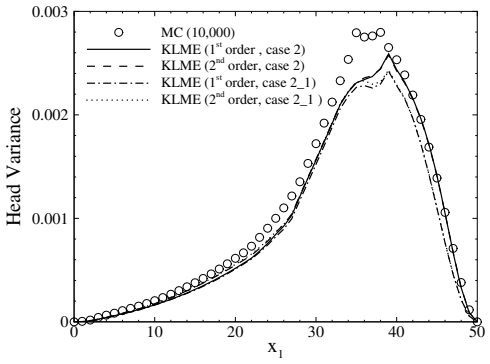

FIG. 5.12. *Comparison of the head variance along the profile* $x_2 = 30$*, computed from MC simulations and the KLME method up to second-order accuracy with* $n_1 = 100$ *(case* 2*) and* $n_1 = 30$ *(case* 2_1*).*

cluded in the decomposition affect the accuracy and efficiency of the KLME method. We also investigate the potential effects of ignoring variability of the log hydraulic conductivity in some zones. Comparing to the base case, case 2, in case 2_1 we reduce the number of modes, n_1, from 100 to 30, while keeping n_2 and n_3 unchanged as in case 2. Since the largest eigenvalue for Zone 3 and Zone 4 is ranked in the sorted set of eigenvalues for the entire domain as 66th and 53rd, respectively, by choosing $n_1 = 30$ we actually have ignored the contribution of parameter variability in these two zones to head variability. Figure 5.12 compares the head variability along a profile $x_2 = 30$, which passes both Zone 3 and Zone 4. The figure clearly indicates that the solutions with only 30 modes in the first-order decomposition can capture the head variability very well, even though 30 modes in the KL decomposition represent only about 50% of the total variability of the log hydraulic conductivity. This phenomenon has been observed earlier [17], although its mechanism is still not clear. Several other observations may be of interest. Although the variability of the hydraulic conductivity in Zones 3 and 4 has been ignored, the head variability in these two zones is nonzero, which means that the head variability is a nonlocal quantity. That is to say, the head variance at any point in the domain depends on variability of the log hydraulic conductivity in the entire domain. In addition, it seems that ignoring variability of hydraulic conductivity in some zones will not significantly affect predicting head

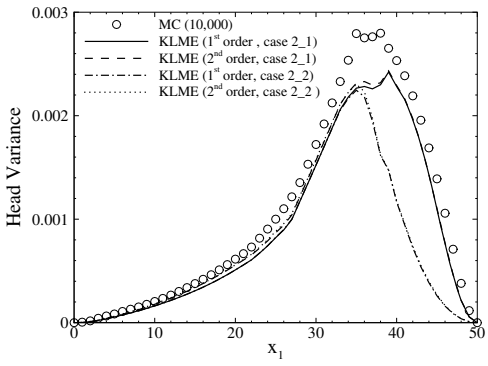

FIG. 5.13. *Comparison of the head variance along the profile* $x_2 = 30$*, computed from MC simulations and the KLME method up to second-order accuracy for case* 2_1 *and case* 2_2.

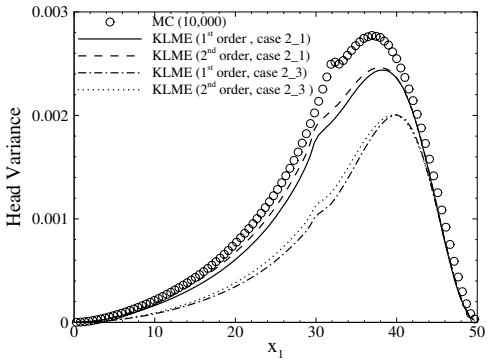

FIG. 5.14. *Comparison of the head variance along the profile* $x_2 = 20$*, computed from MC simulations and the KLME method up to second-order accuracy for case* 2_1 *and case* 2_3.

variability, as long as these zones have either a smaller area or a smaller variability σ_Y^2.

In case 2_1, 30 modes are chosen based on the magnitude of eigenvalues for the entire domain. If instead we choose 30 modes by taking the five largest modes from all six zones (case 2_2), the results from the KLME method will significantly deviate from MC results, as illustrated in Figure 5.13 for the head variance. This comparison indicates that the best strategy for choosing different modes from the decomposition should be based on the magnitude of eigenvalues for the entire domain, which is derived from merging and then sorting eigenvalues of all individual zones, even though potentially this may completely ignore the contribution of variability of the log hydraulic conductivity from some zones.

In contrast to case 2_1, if one ignores the variability of the log hydraulic conductivity in Zone 2, in which both area and variability are large, the results from the KLME method will also deviate significantly from the true solution, as demonstrated in Figure 5.14, where a profile along $x_2 = 20$ compares the head variance derived from MC simulations and the KLME method up to second-order accuracy without

TABLE 5.2
Relative mean squared error of head variance for different cases

Cases	Description	Error of $\sigma_h^{2,[1]}$	Error of $\sigma_h^{2,[2]}$
case 2	$n_1 = 100$	3.49E-02	1.88E-02
case 2_1	$n_1 = 30$ ($\sigma^2_{Y,3}$ and $\sigma^2_{Y,4}$ ignored)	5.41E-02	3.44E-02
case 2_2	$n_1 = 30$ (5 from each zone)	1.26E-01	1.01E-01
case 2_3	$n_1 = 30$ ($\sigma^2_{Y,2}$ ignored)	1.71E-01	1.44E-01

considering σ_Y^2 in Zones 3 and 4 (case 2_1) or without considering σ_Y^2 in Zone 2 (case 2_3).

Figures 5.12–5.14 compare only along a particular profile. To better quantify the error introduced by different strategies for picking modes in the KL decomposition, we calculate the relative mean square error defined as

$$error = \frac{1}{N}\sum_{n=1}^{N}\frac{(u-u_{MC})^2}{u_{MC}^2}, \tag{5.3}$$

where N is the number of grid nodes, u_{MC} is a quantity computed from MC simulations, and u is the corresponding quantity derived from the KLME method. The error measures the average deviation of the KLME solution from the MC results. The errors of computed head variance up to second-order approximations for different cases are listed in Table 5.2, where $\sigma_h^{2,[1]}$ and $\sigma_h^{2,[2]}$ stand for the head variance up to first-order and second-order accuracy, respectively. The table shows that the second-order solution of the head variance is consistently better than the first-order solution. In addition, reducing the number of modes (from 100 to 30) does increase the error. However, given the same number of modes ($n_1 = 30$), choosing modes based on the magnitude of eigenvalues for the entire domain is a better strategy (case 2_1), as compared to the large errors introduced in cases 2_2 and 2_3.

6. Summary and discussions. In this study, we present a methodology for simulating flow in nonstationary permeability fields using the KL-based moment-equation method. The basis of the KLME method is the decomposition of the stochastic permeability field, which involves solving eigenvalues and eigenfunctions of covariance function of the permeability field. In a few special cases, such a decomposition can be done analytically, but, in general, this has to be done numerically, which is computationally expensive for larger-scale problems. When the permeability field is nonstationary, which is a rule rather than an exception, the field in each individual zone can be decomposed separately, and eigenvalues for the entire domain can be obtained by merging eigenvalues from all zones and sorting them in a nondecreasing order, and the eigenfunctions corresponding to the sorted set of eigenvalues for the domain should then be rearranged accordingly.

Once the permeability field is decomposed, the solution process is identical to that presented in [21], and the computational efficiency of the KLME method is still retained. The numerical examples show that, with adequate accuracy, the KLME method is computationally much more efficient than both MC simulations and the CME methods.

The contribution of variability of the log hydraulic conductivity to head moments is related to the product of the subdomain size and its (mean-removed) variability in the log hydraulic conductivity. The numerical experiments demonstrate that the

contribution of the variability in the log hydraulic conductivity from a subdomain after taking into account its mean may be ignored if either this subdomain is small compared to the entire domain or the variability of the log hydraulic conductivity in the subdomain is relatively small. Otherwise, as illustrated in case 2_3, the variability in that zone should be taken into consideration. An important implication is that, in reality, if there is not enough data to infer the variability of the permeability field from a relatively small zone, it may be treated as a deterministic zone without significantly affecting the prediction of the head variability.

In the case that the contribution of (mean-removed) variability of the log hydraulic conductivity from some zones can be neglected, the head variability in these zones, in general, is nonzero unless the problem is completely deterministic. This is because the head variability is nonlocal; i.e., its value at any point depends on variability of the log hydraulic conductivity in the entire domain.

REFERENCES

[1] J. Bear, *Dynamics of Fluids in Porous Media*, Dover, New York, 1972.

[2] M. Chen, D. Zhang, A. A. Keller, and Z. Lu, *A stochastic analysis of steady state two-phase flow in heterogeneous media*, Water Resour. Res., 41 (2005), W01016.

[3] M. Chen, A. A. Keller, D. Zhang, Z. Lu, and G. A. Zyvoloski, *A stochastic analysis of transient two-phase flow in heterogeneous porous media*, Water Resour. Res., 42 (2006), W03425.

[4] R. Courant and D. Hilbert, *Methods of Mathematical Physics*, Interscience, New York, 1953.

[5] J. H. Cushman, *The Physics of Fluids in Hierarchical Porous Media: Angstroms to Miles*, Kluwer Academic Publishers, Norwell, MA, 1997.

[6] G. Dagan, *Flow and Transport in Porous Formations*, Springer-Verlag, New York, 1989.

[7] L. W. Gelhar, *Stochastic Subsurface Hydrology*, Prentice–Hall, Englewood Cliffs, NJ, 1993.

[8] R. Ghanem and P. D. Spanos, *Stochastic Finite Elements: A Spectral Approach*, Springer-Verlag, New York, 1991.

[9] R. Ghanem, *Scale of fluctuation and the propagation of uncertainty in random porous media*, Water Resour. Res., 34 (1998), pp. 2123–2136.

[10] R. Ghanem and S. Dham, *Stochastic finite element analysis for multiphase flow in heterogeneous porous media*, Transp. Porous Media, 32 (1998), pp. 239–262.

[11] G. Liu, D. Zhang, and Z. Lu, *Stochastic uncertainty analysis for unconfined flow systems*, Water Resour. Res., 42 (2006), W09412.

[12] G. Liu, Z. Lu, and D. Zhang, *Stochastic uncertainty analysis for solute transport in randomly heterogeneous media using a Karhunen-Loeve based moment equation approach*, Water Resour. Res., submitted.

[13] M. Loève, *Probability Theory*, 4th ed., Springer-Verlag, Berlin, 1977.

[14] Z. Lu and D. Zhang, *On stochastic modeling of flow in multimodal heterogeneous formations*, Water Resour. Res., 38 (2002), 1190.

[15] Z. Lu and D. Zhang, *A comparative study on flow in uncertainty quantification for heterogeneous media using Monte Carlo simulations randomly conventional and KL-based moment-equation approaches*, SIAM J. Sci. Comput., 26 (2004), pp 558–577.

[16] Z. Lu and D. Zhang, *Conditional simulations of flow in randomly heterogeneous porous media using a KL-based moment-equation approach*, Adv. in Water Resour., 27 (2004), pp. 859–874.

[17] Z. Lu and D. Zhang, *Accurate, efficient quantification of uncertainty for flow in heterogeneous reservoirs using the KLME approach*, SPE J., 11 (2006), pp. 239–247.

[18] Y. Rubin and A. G. Journel, *Simulation of non-Gaussian space random functions for modeling transport in groundwater*, Water Resour. Res., 27 (1991), pp. 1711–1721.

[19] J. Yang, D. Zhang, and Z. Lu, *Stochastic analysis of saturated-unsaturated flow in heterogeneous media by combining Karhunen-Loeve expansion and perturbation method*, J. Hydrology, 294 (2004), pp. 18–38.

[20] D. Zhang, *Stochastic Methods for Flow in Porous Media: Coping with Uncertainties*, Academic Press, San Diego, 2002.

[21] D. Zhang and Z. Lu, *An efficient, high-order perturbation approach for flow in random porous media via Karhunen-Loève and polynomial expansions*, J. Comput. Phys., 194 (2004), pp. 773–794.